

The blue light indicator in rubidium 5S–5P–5D cascade excitation

Waseem Raja¹ · Md. Sabir Ali² · Alok Chakrabarti² · Ayan Ray² 

Received: 6 February 2017 / Accepted: 19 June 2017 / Published online: 23 June 2017
© Springer-Verlag GmbH Germany 2017

Abstract The cascade system has played an important role in contemporary research areas related to fields like Rydberg excitation, four wave mixing and non-classical light generation, etc. Depending on the specific objective, co or counter propagating pump–probe laser experimental geometry is followed. However, the stepwise excitation of atoms to states higher than the first excited state deals with increasingly much fewer number of atoms even compared to the population at first excited level. Hence, one needs a practical indicator to study the complex photon–atom interaction of the cascade system. Here, we experimentally analyze the case of rubidium $5S \rightarrow 5P \rightarrow 5D$ as a specimen of two-step excitation and highlight the efficacy of monitoring one branch, which emits ~ 420 nm, of associated cascade decay route $5D \rightarrow 6P \rightarrow 5S$, as an effective monitor of the coherence in the system.

1 Introduction

The cascade type scheme of atom excitation has remained in the center stage of many important research activities such as multi-step photon–atom interaction [1], study of different aspects of electromagnetically induced transparency [2, 3], Rydberg level spectroscopy [4], four wave mixing (FWM) [5, 6] and related generation of non-classical light [7]. Broadly, the experimental pump–probe

configurations can be subdivided into two categories depending on the specific end goals: (I) counter-propagating (CTP; for EIT and related experiments) and (II) co-propagating (CP; for four wave mixing and related experiments). It has remained a serious concern in all these experiments to find out a marker for monitoring the coherence in the medium. The detection of the absorption/transmission spectra, the fluorescence signal due to spontaneous decay, etc. serve this purpose. However, the absorption/transmission signal is highly weighted by the physical factors like hyperfine transition strength, associated branching ratio (η), relative detuning (Δ) and Rabi frequency (Ω) of the laser, etc. and so do the fluorescence directly associated with the excitation channels. This issue raises a concern for both nearly matched [8] and non-matched wavelength cascade excitations [9] and it requires serious effort to interpret the experimental results with the help of rigorous theoretical calculations.

In the current work, we explore an alternative way to explain the results obtained with our experiments. A test system of nearly same wavelength cascade excitation ($5S_{1/2} \rightarrow 5P_{3/2} \rightarrow 5D_{5/2}$ level scheme of ^{87}Rb) is taken as test bed and different pump–probe geometries have been used with it. Under the CTP geometry Banacloche et al. [2] observed and studied EIT. Later on, Moon et al. [10] further extended the study to conclude that the EIT in a cascade system is associated with double resonance optical pumping (DROP) or two-photon absorption (TPA) background depending on the closed/open nature of the excitation channels. On the other hand, experiments on FWM, non-classical light, stimulated emission [11], etc. are conducted with the help of CP geometry. The complex nature of atom–photon coupling under the cascade level scheme involves absorption, coherence, decay, etc. The last one is an important factor responsible for populating atomic levels even

✉ Ayan Ray
ayan_ray_in@rediffmail.com

¹ Department of Physics, University of Kashmir, Hazratbal, Srinagar 190006, India

² Radioactive Ion Beam Group, Variable Energy Cyclotron Centre, Kolkata 700 064, India

outside the coupling scheme and the decay (fluorescence) associated with such levels can serve as a direct indicator of the relative population at upper levels. Since standard density matrix description of atom–light interaction deals with population elements at the very first level, the information obtained from the fluorescence will, in principle, lead to direct estimation of population and coherence. There exists a cascade decay channel $5D_{5/2} \rightarrow 6P_{3/2} \rightarrow 5S_{1/2}$ [12, 13] with our test system. We present the blue fluorescence originating from $6P_{3/2} \rightarrow 5S_{1/2}$, which is easier to detect, as a possible monitor of population and coherence in case of both CTP and CP geometry. For this purpose, we explore its efficacy in helping us to understand the system better.

We have pursued the experimental study in the way as follows: (i) for CTP geometry the absorption/transmission results are presented with simultaneous recording of blue light and the result is qualitatively explained, (ii) for CP geometry a photon counting measurement is made with the same blue fluorescence and the evolution of frequency count of the data is presented to highlight the onset of coherence in the system.

2 The excitation: decay processes in cascade system and blue light

We consider here the case of building up of population in the $5D_{5/2}$ (Fig. 1) level due to cascade excitation $5S_{1/2} \rightarrow 5P_{3/2} \rightarrow 5D_{5/2}$ of ^{87}Rb . Atoms can reach the uppermost level by two channels: (i) two-photon transition and (ii) two step excitation. Considering the pump(probe) Rabi frequency as $\Omega_{\text{pu}}(\Omega_{\text{pr}})$, we can simply state that the population transfer to $5D_{5/2}$ due to channel (i) is proportional to $\Omega_{\text{pu}}\Omega_{\text{pr}}$ whereas it is proportional to $\Omega_{\text{pu}}\Omega_{\text{pr}}^3$ for channel (ii) [14]. Experiments where the condition is $\Omega_{\text{pu}} \gg \Omega_{\text{pr}}$, (i) are more important whereas (ii) dominates when the system is driven with a strong probe intensity. The phasor diagram presenting the relative competition between (i) and (ii) was reported earlier [14]. According to it on double resonance condition (i) and (ii) are exactly out of phase. For a typical experiment, it is possible to maintain $\Omega_{\text{pr}} \leq \Omega_{\text{sat}}$ and $\Omega_{\text{pr}} \ll \Omega_{\text{pu}}$. In such case, the coherence (ρ_{31}) between $|3\rangle$ and $|1\rangle$ (cf. Fig. 1) is mainly due to two-photon contribution. Here, Ω_{sat} is the Rabi frequency corresponding to saturation intensity $I_{\text{sat}5S_{1/2} \rightarrow 5P_{3/2}}$. In effect monitoring, the population at $5D_{5/2}$ level will help monitoring the two-photon process. We can write ρ_{21}, ρ_{31} as follows [2, 15]:

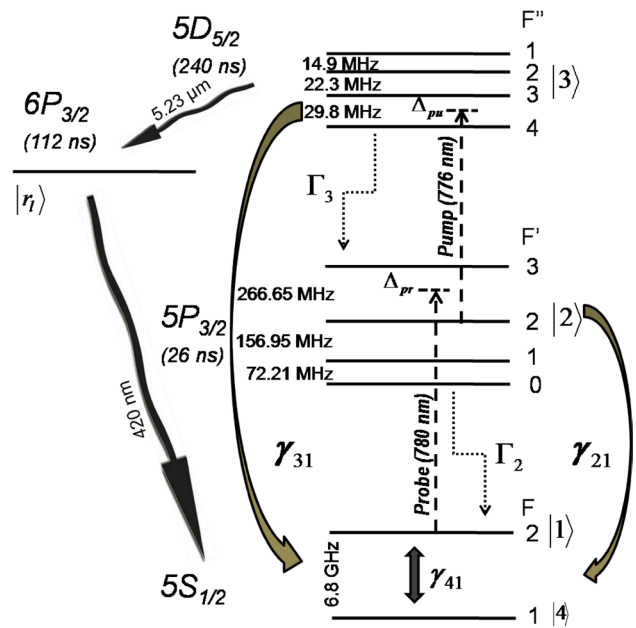


Fig. 1 Level scheme in $5S_{1/2} \rightarrow 5P_{3/2}(D_2) \rightarrow 5D_{5/2}$ transition of Rubidium atom (^{87}Rb), relevant for experiments. The pump (probe) laser beams are linearly polarized. Dephasing between ground states ($|1\rangle \leftrightarrow |4\rangle$) hyperfine components ($F = 2, 1$) is γ_{41} , governed by the transit time broadening. Spontaneous decay rate from $|j\rangle$ is Γ_j (dotted arrows). Here, $\Gamma_3 = 2\pi \times 0.97$ MHz, $\Gamma_2 = 2\pi \times 6.066$ MHz, $\Gamma_1 = 0$ are the natural linewidths. The coherent dephasing rate $|j\rangle \rightarrow |i\rangle$ is $\gamma_{ji} = (\Gamma_j + \Gamma_i)/2$. The decay route $6P_{3/2} \rightarrow 5S_{1/2}$ is used to monitor coherence. Lifetimes of states are also mentioned below respective level captions. The pump (probe) laser frequency detuning and Rabi frequency are $\Delta_{\text{pu}}(\Delta_{\text{pr}})$ and $\Omega_{\text{pu}}(\Omega_{\text{pr}})$, respectively. The two-photon resonance condition is where $\Delta_{\text{pu}} + \Delta_{\text{pr}} \approx 0$; $\Delta_{\text{pu}}(\Delta_{\text{pr}})$ are same as of Ref. [2]

$$\rho_{31} \approx \frac{-i(\Omega_{\text{pu}}/2)}{\gamma_{31} - i(\Delta_{\text{pr}} + \Delta_{\text{pu}})} \rho_{21} \tag{1b}$$

where $\Delta_{\text{pr}} = \omega_{\text{pr}} - \omega_{21}(\Delta_{\text{pu}} = \omega_{\text{pu}} - \omega_{32})$ are detunings of pump(probe) lasers, $\omega_{\text{pr}}(\omega_{\text{pu}})$ are frequencies of probe(pump) laser, and γ_{ji} is the coherence decay rate $(\Gamma_j + \Gamma_i)/2$ for $|i\rangle \rightarrow |j\rangle$ transition. Here, B_j is the line intensity of $F'_j \rightarrow F''$ second excited state hyperfine transitions from j th hyperfine component of first excited state. Also, δ_j denotes the j th energy gap between F'' hyperfine levels as measured from $F'' = 4$ position and the probe laser absorption is proportional to $\text{Im}(\rho_{21})$ (cf. Eq. 1a). After averaging over the Maxwell–Boltzmann velocity distribution of the Doppler broadened atomic system, $\text{Im}(\rho_{21})$ versus Δ_{pr} plot (Fig. 2a) shows the probe absorption, which is modified by

$$\rho_{21} \approx \frac{i(\Omega_{\text{pr}}/2)}{\gamma_{21} - i\Delta_{\text{pr}} + \frac{\Omega_{\text{pu}}^2}{4(\sum_{j=1}^3 B_j)}} \left[B_1 \{ \gamma_{31} - i(\Delta_{\text{pr}} + \Delta_{\text{pu}} + \delta_1) \}^{-1} + B_2 \{ \gamma_{31} - i(\Delta_{\text{pr}} + \Delta_{\text{pu}} + \delta_2) \}^{-1} + B_3 \{ \gamma_{31} - i(\Delta_{\text{pr}} + \Delta_{\text{pu}} + \delta_3) \}^{-1} \right] \tag{1a}$$

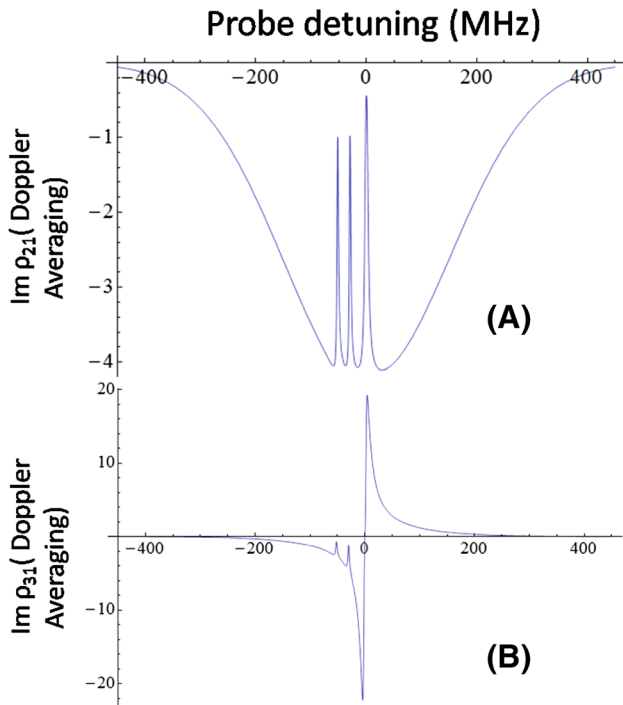


Fig. 2 Result of: **a** theoretical calculation of Doppler averaged $\text{Im}(\rho_{21})$ versus Δ_{pr} for cascade system. Under CTP condition, the relative strengths of DROP signals are determined experimentally ($\sim 1.0:0.42:0.40$) with pump scanning and probe stabilized on $F = 2 \rightarrow F' = 3$ condition. **b** Calculation of Doppler averaged $\text{Im}(\rho_{31})$ versus Δ_{pr} shows the velocity selective character of coherence between dipole forbidden states, i.e., $|1\rangle \rightarrow |3\rangle$. Here, experimental values of $\Omega_{\text{pr}}(\Omega_{\text{pu}}) \sim 2\pi \times 10$ ($\sim 2\pi \times 70$) MHz and Doppler width 560 MHz (at room temperature) are used in calculation to replicate experimental situation

the presence of pump field connecting $|2\rangle \rightarrow |3\rangle$ [15], i.e., $F' = 2 \rightarrow F'' = 4,3,2$ in our case (cf. Fig. 1). Experimentally determined relative line intensity (B_i) values are used here. In this case, only lowest order contribution from probe laser is taken into account because $\Omega_{\text{pu}} \gg \Omega_{\text{pr}}$. We consider the specific case of Rb atom (see Fig. 1) where $(\omega_{\text{pu}} - \omega_{\text{pr}})/\omega_0 \ll 1$; ω_0 is the nominal frequency of the atomic transition ($\sim 2\pi \times 384.23$ THz in air for ^{87}Rb D_2 transition). Figure 2b shows Doppler averaged $\text{Im}(\rho_{31})$ versus Δ_{pr} plot depicting the velocity selective nature of coherence between dipole forbidden states in cascade excitation (cf. Eq. 1b).

$\lim_{\gamma_{31} \rightarrow 0}$ The excitation channel $5S_{1/2}(F = 2) \rightarrow 5P_{3/2}(F') \rightarrow 5D_{5/2}(F'')$ indicates that there remains finite chance so that atoms can decay to uncoupled state $F = 1$ due to Γ_3 and Γ_2 (Fig. 1). Except γ_{41} (determined by transit time broadening; $2\pi \times 0.05$ MHz

in the present case), which is slow in nature, no other mechanism is present for $F = 1 \leftrightarrow 2$ population transfer. The atoms at $F = 1$ are temporarily lost from excitation-decay cycle. As a result, we see the DROP in transmission signal and it is indeed the measure of TPA. Under the CTP geometry, EIT appears as a fine structure within the DROP background due to destructive interference between excitation pathways. However, strong EIT condition demands, i.e., virtually no loss of population to $F = 1$ state. But this is not the case in actual practice. Hence, EIT is often masked under DROP background except largely detuned conditions [16, 17]. Under CP geometry, the EIT is not seen but TPA results are same as that of CTP.

The cascade decay route of our interest is $5D_{5/2} \rightarrow 6P_{3/2} \rightarrow 5S_{1/2}$. The life times (τ) are in order: $\tau_{5P_{3/2}}(26 \text{ ns}) < \tau_{6P_{3/2}}(112 \text{ ns}) < \tau_{5D_{5/2}}(240 \text{ ns})$. Effectively $6P_{3/2}$, which is decoupled from the excitation channels, acts as a reservoir $|r_1\rangle$ w.r.t $5P_{3/2}$ with leakage rate slow enough satisfying $\tau_{6P_{3/2}} \sim 5\tau_{5P_{3/2}}$. On the other hand, $\tau_{6P_{3/2}} < 0.5\tau_{5D_{5/2}}$; hence spontaneous emission $6P_{3/2} \rightarrow 5S_{1/2}$ can replicate hyperfine structure of $5D_{5/2}$ level (cf. Fig. 1a) [18]. The line intensity of the blue fluorescence can directly (weighted only by η) provide information about the population history. Further in a simplistic way, it is possible to operate under conditions: $I_{\text{pu}} \geq I_{\text{sat}5P_{3/2} \rightarrow 5D_{5/2}}, I_{\text{pr}} \leq I_{\text{sat}5S_{1/2} \rightarrow 5P_{3/2}}$; hence, the blue light intensity (I_{blue}) may bear a correlation with I_{pr} . It shows that there exists finite possibility to produce spontaneous emission in a cascade decay, which at least can be made intensity correlated to the probe. Here, $I_{\text{pr}}(I_{\text{pu}})$ is intensity of probe(pump) laser and is proportional to $\Omega_{\text{pu}}^2(\Omega_{\text{pr}}^2)$. Under two level approximation, Ω and I are connected by: $\Omega \approx 2.2 \times 10^8 \text{ s}^{-1} \times \sqrt{I(\text{Wcm}^{-2})} \times D$ [19], where D is the dipole moment of the transition in atomic unit.

By considering the spontaneous emission as quantized, the two-photon cascade decay ($|3\rangle \rightarrow |r_1\rangle \rightarrow |1\rangle$) may be understood as follows: (i) initially, the atom occupies the highest excited state $|3\rangle$ (cf. Fig. 1) while the field remains in vacuum $|0\rangle$, (ii) the excited atom decays to intermediate state $|r_1\rangle$ by emitting a photon and makes a final move to $|1\rangle$ with emission of another photon. The total state vector is a linear superposition of all possible atom–field product states. Considering $\vec{r}_o(\vec{k}_i)$ as the initial position vector of the atom emitter (wavevector of the i th photon), the radiation field $|\gamma, \phi\rangle$ in case of a cascade two-photon emitter may be ideally expressed as [16]:

$$|\gamma, \phi\rangle = - \sum_{\vec{k}_1, \vec{k}_2} \frac{g_{3, \vec{k}_1} g_{r_1, \vec{k}_2} e^{-i(\vec{k}_1 + \vec{k}_2) \cdot \vec{r}_o}}{[i(\omega_{k_1} + \omega_{k_2} - \omega_{31}) - \gamma_{3r_1}][i(\omega_{k_2} - \omega_{r_1}) - \gamma_{r_1 1}]} |1_{\vec{k}_1}, 1_{\vec{k}_2}\rangle \quad (2)$$

Here, $|1_{\vec{k}_1}, 1_{\vec{k}_2}\rangle$ is the two-photon state vector and it is not possible to distinguish between the photon emission sequences like $|3\rangle \rightarrow |r_1\rangle$ followed by $|r_1\rangle \rightarrow |1\rangle$ or vice versa. Hence, Eq. 2 indicates the inseparability of the emitted photons from cascade emitter. Since initial and final states are well determined, according to Feynmann's rule the two individual decay amplitudes ($g_{i,\vec{k}}$) need to be coherently added to find out the transition probability of $|3\rangle \rightarrow |1\rangle$ [20]. It is to be noted that 'g's in fully quantum description (cf. Eq. 2) of the system are similar to that of Ω (Rabi frequency), which is used in semi-classical treatment. For cascade emitter of Fig. 1, i.e., $|3\rangle \rightarrow |r_1\rangle \rightarrow |1\rangle$ the values of wave vectors are: $2\pi/5.23 \mu\text{m}$ and $2\pi/420 \text{ nm}$.

It is a fact that coherent light is changed into sub-Poissonian light (non-classical characteristics) after the interaction with the two-photon absorbers and it acquires some amount of squeezing [21]. The squeezed state is

identical to the two-photon coherent state introduced by Yuen [22]. The two-photon coherent state is related to conventional coherent state through a unitary transformation but exhibits photon statistics different from that of coherent state. Since the connection between the cascade emitter and the two-photon coherent state is close but not so straightforward in nature, it is worthwhile to explore the counting of the blue fluorescence photons (with overlapping pump-probe sequence) as a measure to monitor the evolution of the cascade decay process towards ideal two-photon coherent state. The squeezing of spontaneous emission fluctuations in a single three-level atom originates from preparation of coherent superposition of ground state ($|1\rangle$) and topmost state ($|3\rangle$) [23]. Here, we will present the blue photon distribution function as a preliminary measure of the changing character of the coherence in the cascade emitter.

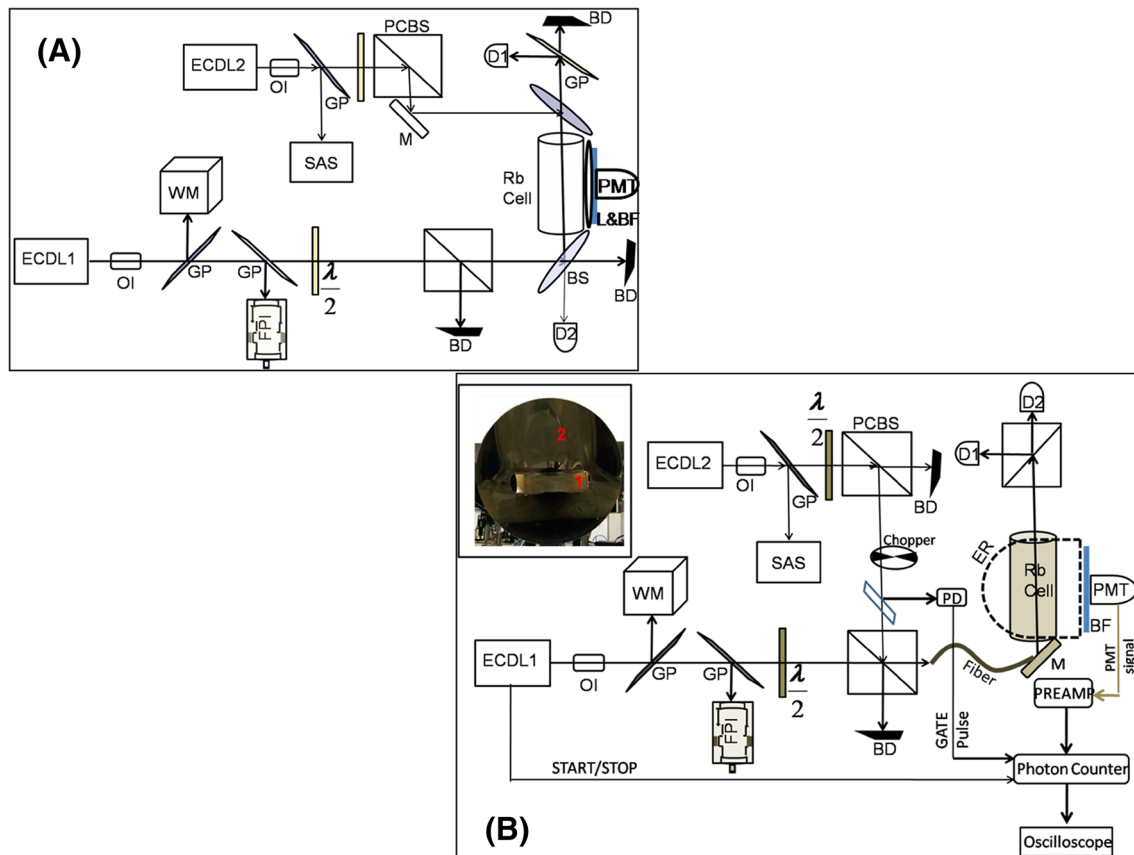


Fig. 3 Schematic of the experimental arrangements of pump-probe geometry: **a** counter-propagating, **b** co-propagating. Here, *ECDL1(2)* pump(probe) external cavity diode lasers, *OI* optical isolator, *M* mirror, *BS* beam splitter, *PCBS* polarizing cube beam splitter, *BD* beam dump, *PD* photodetector (for other use), *D* photodetector (for measuring transmission), $\lambda/2$ half waveplate, *FPI* Fabry-Perot interferometer, *WM* wavemeter, *GP* glass plate, *L* collimating lens, *BF* blue fil-

ter, *PMT* photomultiplier tube, *ER* ellipsoid reflector, *SAS* saturation absorption spectroscopy, *PREAMP* preamplifier (SR445A, Stanford Research), and *OSC* oscilloscope. Here, SR400 gated photon counter is used. *Inset* of **(b)** shows the actual positioning of (1) Rb vapor cell inside the (2) ellipsoid reflector (REM-144.2-31.8-21.0, CVI Melles Griot)

3 Experiment

Two single mode tunable external cavity diode lasers are used in pump (emitting ~ 776 nm; $5P_{3/2} \rightarrow 5D_{5/2}$)-probe (emitting 780 nm; $5S_{1/2} \rightarrow 5P_{3/2}$) configuration in an Rb vapor cell (without buffer gas) maintained at room temperature (see Fig. 3). Both the beams are plane polarized. In one geometry, the probe laser counter-propagates the pump (*cf.* Fig. 3a, CTP), while in the other configuration (*cf.* Fig. 3b, CP) they co-propagate. Under both arrangements, the emitted blue light is monitored with a photomultiplier tube (PMT) preceded by a blue filter. Specially for CP geometry ($I_{\text{pr(pu)}} \ll I_{\text{sat}5S_{1/2} \rightarrow 5P_{3/2}}(5P_{3/2} \rightarrow 5D_{5/2})$), we placed the Rb vapor cell at the first focus of an ellipsoid reflector and the PMT is placed at the second focus. The inset of Fig. 3b shows the actual situation when the cell is housed in the reflector. A synchronous photon counting scheme (Fig. 3b) is followed for CP geometry to study the blue fluorescence. A mechanical chopper is used to supply GATE pulse, whereas the laser scan trigger pulse is used for photon counting START/STOP sequence. During experiment, the pump laser is in resonance with $F' = 3 \rightarrow F'' = 4,3,2$ hyperfine domain, while the probe laser is resonant with $F = 2 \rightarrow F' = 3$ component to complete cascade scheme. Since energy gap ($\Delta E_{F'=3 \rightarrow F''}$) between hyperfine components $F' = 3 \rightarrow F''$ is very close compared to that of $F = 2 \rightarrow F'$ ($\Delta E_{F=2 \rightarrow F'}$), the influence of pump laser is evident on all F'' components. The frequency scale is calibrated with the help of probe saturation absorption spectrum (SAS). Also, a wavemeter and a scanning Fabry–Perot Etalon are used for monitoring the pump/probe laser frequency scan.

4 Results and discussion

To adjust the laser parameters, we consider effective dipole moments (in a.u.): $D_{5S_{1/2}(F=2) \rightarrow 5P_{3/2}(F'=3)} = 2.042$ [24] and $D_{5P_{3/2} \rightarrow 5D_{5/2}} = 2.334$ [25, 26] for linear polarization. For CTP geometry, a combination of probe(pump) laser power of $500 \mu\text{W}$ (20 mW), which we estimate as $\Omega_{\text{pr}}(\Omega_{\text{pu}}) \sim 2\pi \times 10$ ($\sim 2\pi \times 70$) MHz, is used.

Under CTP pump–probe geometry, it can be seen from different plots (Fig. 4a, c) that the observed DROP signals reside on a flat background for particular value of ω_{pr} (stabilized to SAS signals of $|1\rangle \rightarrow |2\rangle$). The pump laser in principle addresses small velocity groups of atoms resonant with ω_{pr} . Due to the participation of highly selective velocity groups of atoms, the resultant Doppler background is almost absent. However, under ω_{pr} scanning condition (see inset plots of Fig. 4) much larger velocity groups of atoms are involved giving rise to Doppler

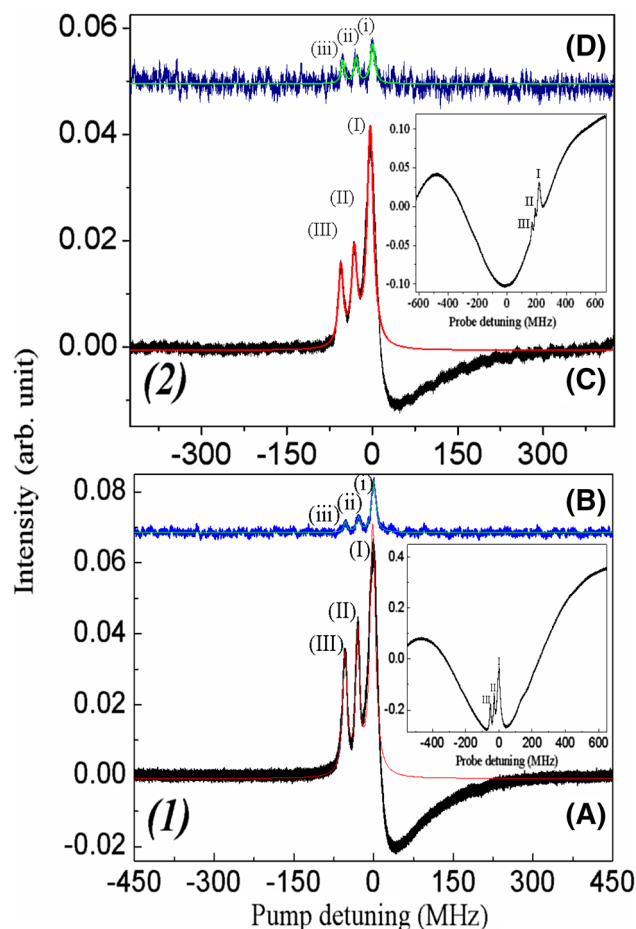


Fig. 4 Results of counter-propagating pump–probe geometry: (I) DROP (a) and corresponding blue fluorescence (b) spectra for resonant cascade level coupling of $F = 2 \rightarrow F' = 3 \rightarrow F'' = 4,3,2$ transition manifold. (2) DROP (c) and respective blue fluorescence (d) spectra for the same under off-resonant coupling, i.e., $F = 2 \rightarrow F' = 3,1(\text{crossover}) \rightarrow F''$. Note here that EIT is seen on DROP under off-resonance when $F = 2 \rightarrow F' \rightarrow F''$ coupling is further red detuned from $F' = 3,1(\text{crossover})$ intermediate state [16]. Also {(I), (II), (III)} denote DROP components corresponding to two-photon absorption $F = 2 \rightarrow F'' = 4,3,2$ under on- and off-resonant conditions. The blue fluorescence peaks are denoted by {(i), (ii), (iii)} in both cases. The Red and Green lines are results of Lorentzian multi-peak fitting to DROP and blue peaks. The fitting results are tabulated in Table 1. Here, $\Omega_{\text{pr}}(\Omega_{\text{pu}}) \sim 2\pi \times 10(70)$ MHz are used. Insets of (1) and (2) show the DROP spectra under probe scanning, pump stabilized condition for On and Off-resonant cases

background. For Fig. 4a, c the probe–pump combination satisfies conditions: 1. ($F = 2 \rightarrow F' = 3 \rightarrow F''$, i.e., almost perfect two-photon resonance condition $\Delta_{\text{pu}} + \Delta_{\text{pr}} \approx 0$ and $\Delta_{\text{pu}} \approx 0 \approx \Delta_{\text{pr}}$), 2. ($F = 2 \rightarrow \text{crossover } F' = 3, 1 \rightarrow F''$, i.e., mere two photon resonance $\Delta_{\text{pu}} + \Delta_{\text{pr}} \approx 0$ but $\Delta_{\text{pu}} \neq 0 \neq \Delta_{\text{pr}}$). For perfect two-photon resonance ($F = 2 \rightarrow F' = 3 \rightarrow F'' = 4$), the decay route $F'' = 4$ (branching ratio $\eta = 0.76$) $\rightarrow F' = 3$ ($\eta = 1$) $\rightarrow F = 2$ forms a pseudo-closed absorption–emission cycle.

However, due to velocity selective nature of generalized Rabi frequency ($\sqrt{\Omega^2 + \Delta^2}$; $\Delta = kv$), it is apparent that other decay routes are also present there to sufficiently populate $F = 1$ state. This condition facilitates DROP and the signature of EIT is almost obscured. Here, v is the velocity of atom. Except the variation in relative line strengths, the observation of DROP is similar in case of both perfect and mere two photon resonance conditions. Only the signature of EIT has become little more visible on the tip of the strongest DROP component. These two conditions (*cf.* Fig. 4) are willfully chosen for experiment because we wanted to avoid the influence of EIT as it hinders TPA. The experimental observations are in accordance with our earlier reports [16, 17] verifying that the condition of loss of atoms from $F = 2 \rightarrow F' \rightarrow F''$ cycle to $F = 1$ is strongly satisfied. Ideal EIT condition demands no loss of atoms, which is strongly violated here. Thereby, the EIT effect is considerably weakened.

The recorded blue fluorescence spectra under above-mentioned conditions, i.e., 1 and 2 are presented in Fig. 4b, d. The blue light peaks (i), (ii), (iii) correspond to DROP peaks (I), (II), (III). Here (I), (II), (III) correspond to two photon transitions $F = 2 \rightarrow F'' = 4, 3, 2$. Hence, the blue light effectively maps the hyperfine manifold of $5D_{5/2}$ level. The DROP and blue light peaks are fitted to standard Lorentzian multi-peak fitting profile and Table 1 shows the results. The theoretical width $\Gamma_{\text{DROP}, J}$ [27] of individual DROP component is: $(\omega_{\text{pu}}/\omega_{\text{pr}})(\Gamma_2 + \Gamma_3) + \sum_{i=1,2} \Delta v_i$ (8.5 MHz). Here, contribution of laser linewidth is $\Sigma \Delta v_{\text{laser}} \sim 2$ MHz. Other major contributors are: residual Doppler broadening (~ 3 MHz) [18], transit time broadening (0.05 MHz) and optical misalignment. Similarly width $\Gamma_{\text{blue}, k}$ of individual blue line peaks are primarily limited by natural linewidth $2\pi \times 1.3$ MHz [18] and other factors as mentioned above. Here, experimental values of $\Gamma_{\text{DROP}, J}$ and $\Gamma_{\text{blue}, K}$ closely match with the estimation (see Table 1). Also $\Gamma_{\text{blue}, K}$ follows the similar descending order of $\Gamma_{\text{DROP}, J}$ except a variation in $J = \text{II}(k = \text{ii})$ for Fig. 4a, b. The variation may have come due to incoherent pumping and related velocity thermalization effect [18]. We now consider the linestrengths of DROP and blue light peaks. The order of relative linestrengths of $\text{cascade}_{\text{DROP}, J}$ components is in agreement with $\text{cascade}_{\text{blue}, k}$ components for both cases of Figs. 4a, b and c, d. Since linestrength of DROP is proportional to that of TPA [10], the blue fluorescence peaks provide an in-depth information about the two-photon process residing in the medium. The EIT, on the other hand, reduces TPA. Hence, EIT on DROP background (becomes more prominent with stronger satisfaction of mere two-photon resonance condition, which is discussed earlier) is marked by increasingly weaker blue fluorescence as it originates from decay of population through $5D_{5/2} \rightarrow 6P_{3/2} \rightarrow 5S_{1/2}$ route. Since EIT is a result

Table 1 DROP and blue fluorescence statistics of cascade system (*cf.* Fig. 4)

Peak designation etc.	$F = 2 \rightarrow F' = 3 \rightarrow F''$ (exact on-resonance)	$F = 2 \rightarrow F' = 3, 1 \rightarrow F''$ (detuned on-resonance)	Condition (related to Fig. 5)
Fitted blue light peak (F'' marker)	$A_i(F'' = 4)$	$A_i(F'' = 4)$	Here cascade (closed; <i>Exact On-resonance</i>) and cascade (open; <i>Detuned On-resonance</i>) systems are compared. All blue (DROP) spectral strengths are normalized to $A_k(A_j)$ i.e.
Relative intensity ($\text{cascade}_{\text{blue}, k}$), FWHM in MHz ($\Gamma_{\text{blue}, k}$)	$A_{\text{ii}}(F'' = 3)$ 1, 10.02363	$A_{\text{ii}}(F'' = 3)$ 0.236, 8.75435	$A_{\text{iii}}(F'' = 2)$ 0.221, 7.41853
Fitted DROP peak (F'' marker)	$A_i(F'' = 4)$	$A_i(F'' = 4)$	$A_{\text{ii}}(F'' = 2)$ 0.177, 10.25402
Relative intensity ($\text{cascade}_{\text{DROP}, J}$), FWHM in MHz ($\Gamma_{\text{DROP}, J}$)	$A_{\text{ii}}(F'' = 3)$ 1, 12.28097	$A_{\text{ii}}(F'' = 3)$ 0.415, 9.27391	$A_{\text{iii}}(F'' = 2)$ 0.402, 10.37909
Remark	The order of $\text{cascade}_{\text{blue}}$ is same as that of $\text{cascade}_{\text{DROP}}$ under both conditions. Γ values also do show similar order with one exception. However, the observed deviation in normalized values may be attributed to EIT effect, which leads to suppression of TPA. Also responsible is the effect of velocity thermalization due to incoherent optical pumping [18]		

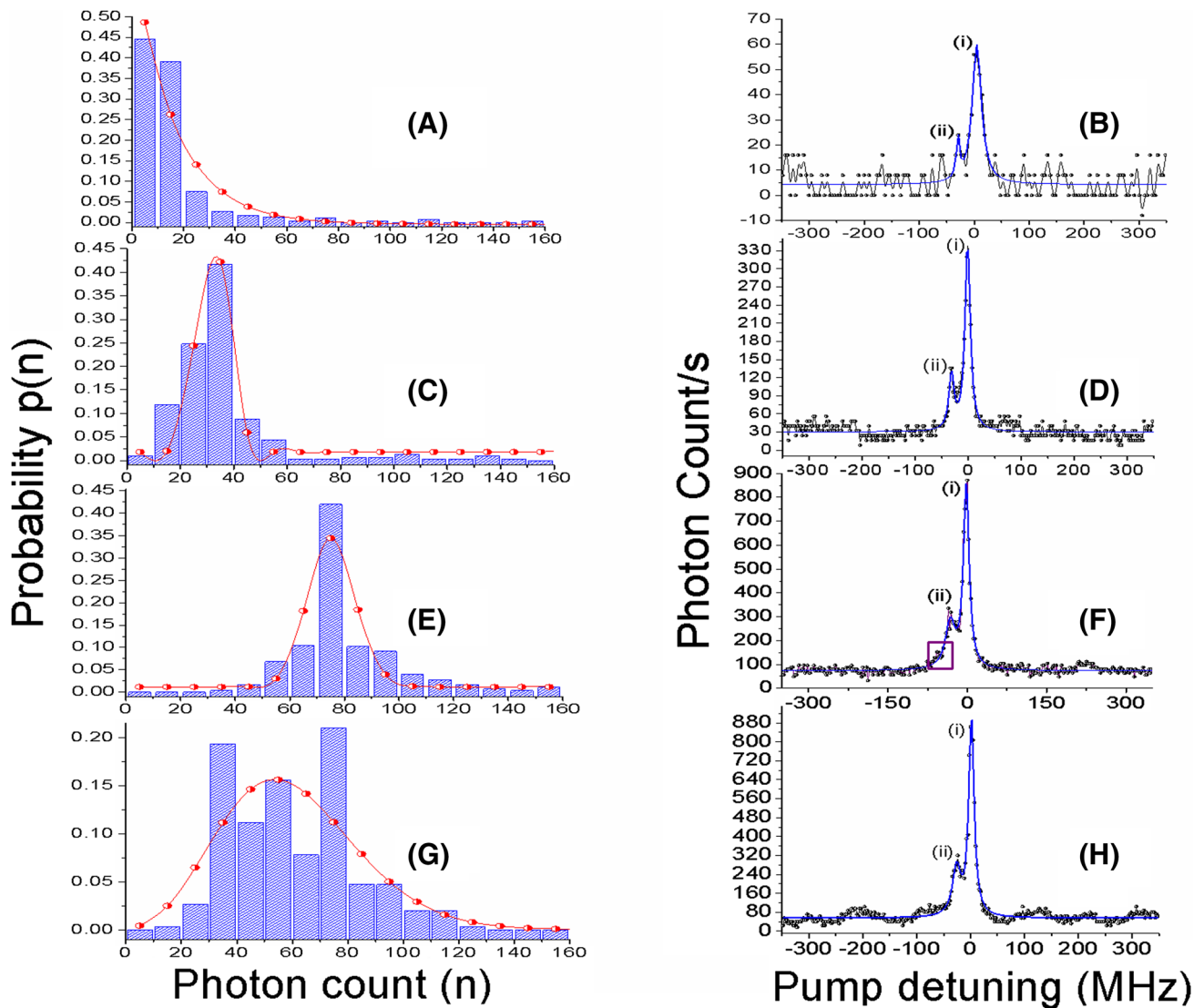


Fig. 5 Results of co-propagating pump–probe geometry: **a**, **c**, **e**, **g** show photon distribution for situations **(b)**, **(d)**, **(f)**, **(h)**. Here, probe–pump combination satisfies resonant cascade level coupling of $F = 2 \rightarrow F' = 3 \rightarrow F'' = 4,3,2$. Here, **{(b), (d), (f)}** present blue fluorescence pertaining to situations of $\Omega_{pu} (\Omega_{pr}) \sim 2\pi \times 9(1.74, 2.2, 2.46, 3.11)$ MHz. The photon distribution in **a** matches with BE statistics representing the quasi-thermal nature of blue light at a very low probe power. With small change in probe power, the distribution tends to become Poissonian **(c)**, **(e)**. The Poissonian distribution shows near constant intensity of blue light. It indicates the formation of individual coherent state but it is uncorrelated. The distribution starts deviating from Poissonian indicating the transformation of cas-

cade emitter system towards the possible formation of a two-photon coherent state, which has been qualitatively analyzed by fitting the data in **g** with a general expression (see text for details). The fitting result indicates sub-Poisson character of the blue light. But alone blue photon distribution is insufficient to predict further about possible existence of sub-Poisson statistics. The red lines represent equivalent Chi square fitting for respective Histograms. The blue lines on **b**, **d**, **f**, **h** show multi-peak Lorentz fit to the two photon spectra. Peaks (i) and (ii) correspond to $F = 2 \rightarrow F'' = 4,3$ two photon transitions, which is further confirmed from fitted linecenters. However, $F = 2 \rightarrow F'' = 2$ is not noticed (due to low value of laser intensity) except in **(F)**, where trace of the component (highlighted) is noticed

of coherence, the observed blue light intensity acts as a measure to mark the onset/obscuring of EIT coherence too. The close connection between blue light intensity and EIT/DROP condition has been reported earlier by us [16].

In case of co-propagating geometry, the pump–probe beams are passed through an optical fiber. This arrangement ensures better satisfaction of phase matching condition:

$\vec{k}_{780\text{nm}} + \vec{k}_{776\text{nm}} = \vec{k}_{5.23\mu\text{m}} + \vec{k}_{420\text{nm}}$ due to better alignment and preserves the polarization of the laser before entering Rb cell. However, we operated at low laser intensity ($\ll I_{\text{sat}}$). A nominal value of $330 \mu\text{W}$ ($3 \rightarrow 130 \mu\text{W}$) is used as $I_{\text{pu}}(I_{\text{pr}})$ where it is easy to conduct photon counting. Also, we operate with relatively less number of atoms (Rb vapor cell at 25°C) ensuring $\lambda_{\text{mean}} \text{freepath} \gg \lambda_{780, 776\text{nm}}$. As

a result, the effect of velocity changing collisions can be ignored. Our measurements are conducted with a sampling time (τ_{samp}) of 100 ms. A typical photon counting sequence starts with laser scan, which lasts for 250 s. According to our experimental scheme, the order of timescale is: $\tau_{5P_{3/2}} < \tau_{6P_{3/2}} < \tau_{5D_{5/2}} \ll \gamma_{41}^{-1} < \tau_{\text{samp}}$. Considering this fact we may state that blue photons are counted under equilibrium condition (e.g., transient events occurring in the timescale of optical pumping Ω^2/Γ [28] are averaged out during each τ_{samp}). Figure 5a, c, e, g shows the results of photon counting under same Ω_{pu} ($2\pi \times 9$ MHz) but different Ω_{pr} $\{2\pi \times (1.74, 2.2, 2.46, 3.11)\text{MHz}\}$ values. On the other hand, Fig. 5b, d, f, h shows the actual blue light spectra where (i) and (ii) indicate two photon transitions $F = 2 \rightarrow F'' = 4, 3$. Due to low value of $I_{\text{pu,pr}}$, the $F = 2 \rightarrow F'' = 2$ component is not resolved in photon counting measurements. The X axis calibration for Fig. 5b, d, f, h is done with the help of Etalon fringes. The identity of peaks (i) and (ii) is verified using the fitted line centers. The X axis of Fig. 5a, c, e, g is the Bin or Photon counts (n) obtained from frequency counting analysis of recorded fluorescence photons data. The Y axis of the same plots presents probability $p(n)$ of the Photon count. The $p(n)$ versus n plot (cf. Fig. 5a) shows the nature dominated by Bose–Einstein (BE) statistics. The red lines show equivalent Chi square fitting [29] of experimental data with theoretical distribution $p(n) = \frac{\langle n \rangle^n}{(1 + \langle n \rangle)^{n+1}}$ [30], where $\langle n \rangle$ is the mean number of photons in the coherent state. At relatively low laser intensity level, the number of blue photons is very low (see Fig. 5b). This is because the resident two-photon coherence and related TPA are very weak and the blue radiation is largely incoherent. So the quasi-thermal character of the blue photons is represented by BE distribution. With increment in I_{pr} the TPA strengthens and the emitted blue light starts to behave as coherent radiation as is evident in Fig. 5c, which when fitted to Poisson distribution exhibits higher residuals compared to that of Fig. 5e. The Poisson statistics is the primary signature of a coherent state. The close resemblance of the blue photon distribution (cf. Fig. 5e) to Poisson statistics indicates constant intensity of the blue light source. However, Fig. 5e at best represents a single coherent state, which is still uncorrelated to the other branch of spontaneous emission ($5D \rightarrow 6P$). On increasing I_{pr} further the blue photon distribution starts to deviate from the Poisson statistics (cf. Fig. 5g). In this case, the emitted radiations start to become correlated and the atom–field system may form a two-photon coherent state. Indeed, it has been shown earlier by Ficek et al. [31] that large squeezing can be traced in fluorescent intensity near two-photon resonance for moderate laser intensity in a cascade system. The photon distribution function of a squeezed state is complex compared to that of a single coherent state

[30]. In a simplistic manner, we may try to characterize the $p(n)$ versus n plot (cf. Fig. 5g) by fitting with a function of the form $p(n) = \frac{\langle n \rangle^n A^{(n/A)} e^{-\langle n \rangle A}}{(n/A)!}$ where the designations are: $A = 1$ (Poisson), $A > 1$ (sub-Poisson) and $A < 1$ (super-Poisson) [32]. Here ‘ A ’, the weight factor and $\langle n \rangle$ both are fitting parameters without any bounds. The fitted value ($A > 1$) indicates the sub-Poisson character of blue light. It suggests that the squeezing may be present in $|\gamma, \varphi\rangle$ of Eq. 2 but is much smaller compared to the coherent component [30] introduced by the detection scheme. It may also be noted that fitted values of $\langle n \rangle$ are different for Fig. 5a, c, e, g. However the above-mentioned qualitative analysis based on sole monitoring of blue light is not enough to confirm the presence of squeezing and requires further higher order correlation measurements to confirm non-classicality of photons. The photon statistics of blue light can at best indicate evolution of the system from an incoherent (quasi-thermal blue light, BE distribution) \rightarrow coherent (Poisson distribution, uncorrelated) \rightarrow two-photon coherent state.

5 Conclusion

The excitation process under cascade level scheme is of great importance as it directly deals with transfer of atoms to higher excited states including Rydberg, auto-ionizing levels or even the continuum. However, it has always remained as the primary aim of research to maximize population at excited states by adjusting the coherence in the atom–field medium. This is indeed extremely important and demands special attention because the cascade scheme is used in many fields already mentioned earlier. In this report, we have taken $^{87}\text{Rb } 5S_{1/2} \rightarrow 5P_{3/2} \rightarrow 5D_{5/2}$ cascade channel as a specimen and propose application of one of the spontaneous radiations at 420 nm emanating from $5D_{5/2} \rightarrow 6P_{3/2} \rightarrow 5S_{1/2}$ decay route as an effective monitor for light–atom interaction in cascade system. By optimizing the blue light intensity (under counter-propagating pump–probe geometry), we can effectively optimize the population at topmost excited level under stepwise excitation process and can move between DROP/EIT coherence conditions. On the other hand, by inspecting the blue photon statistics (under co-propagating geometry) we can predict the evolution of coherence in the cascade medium.

In this regard, we extend our experimental investigation using both semi-classical and full quantum descriptions of the system. Under counter-propagating pump–probe excitation double resonance optical pumping signals, which are proportional to two-photon excitation, are observed. Consequently, blue light peaks are also observed and there remains a correlation between the line parameters for DROP and blue light. Hence by monitoring blue light signal, one may predict

population level at $5D_{5/2}$ state. By minimizing the blue light intensity, one can reduce the loss of atoms from cascade excitation channel. In such case, the system will have strong presence of EIT, which will hinder TPA. On the other hand, maximizing the blue fluorescence will increase effective population at $5D_{5/2}$ level, thereby favoring the TPA process.

Under the full quantum–mechanical description of the system, we studied the photon statistics of blue fluorescence when co-propagating pump–probe geometry is employed. Under the phase matching condition, it is found that the statistical distribution evolves from BE distribution to Poisson distribution marking the transformation of incoherence (quasi-thermal blue light) to coherence (constant intensity of blue light). On further adjustment of laser parameters, it is found that the distribution deviates from the Poisson statistics marking the onset of correlation of spontaneous emission channels. A qualitative analysis is carried out which reveals that sub-Poissonian character may be present in the photon distribution. However, to confirm the presence of squeezing higher order correlation study is required. This is an ongoing work [33] where cross-correlation between excitation and emitted photons need to be studied in details.

We have shown that the blue fluorescence alone can act as an effective handle to study the atom–field interaction in the cascade system. We believe that such kind of approach to study the atom–photon interaction of the system will also be useful for other multi-step excitations. Also, it will help us to predict when the system is nearing to exhibit non-classical behavior.

References

1. V.S. Letokhov, Nonlinear laser chemistry. Springer Ser. Chem. Phys. **22**, 78 (1983)
2. J. Gea-Banacloche, Y. Li, S. Jin, M. Xiao, Phys. Rev. A **51**, 576 (1995)
3. N. Radwell, T.W. Clark, B. Piccirillo, S.M. Barnett, S. Franke-Arnold, Phys. Rev. Lett. **114**, 123603 (2015)
4. D.P. Fahey, M.W. Noel, Opt. Exp. **19**, 17002 (2011)
5. A.M. Akulshin, R.J. McLean, A.I. Sidorov, P. Hannaford, Opt. Exp. **17**, 22861 (2009)
6. G. Walker, A.S. Arnold, S. Franke-Arnold, Phys. Rev. Lett. **108**, 243601 (2012)
7. E. Alebachew, K. Fesseha, Opt. Commun. **265**, 314 (2006)
8. R.R. Moseley, S. Shepherd, D.J. Fulton, B.D. Sinclair, Malcolm H. Dunn, Opt. Commun. **119**, 61 (1995)
9. A. Urvoy, C. Carr, R. Ritter, C.S. Adams, K.J. Weatherill, R. Low, J. Phys. B **46**, 245001 (2013)
10. H.S. Moon, L. Lee, J.B. Kim, Opt. Exp. **16**, 12163 (2008)
11. C.V. Sulham, G.A. Pitz, G.P. Perram, Appl. Phys. B **101**, 57 (2010)
12. T. Meijer, J.D. White, B. Smeets, M. Jeppesen, R.E. Scholten, Opt. Lett. **31**, 1002 (2006)
13. A. Akulshin, C. Perrella, G.W. Truong, R. McLean, A. Luiten, J. Phys. B **45**, 245503 (2012)
14. R.R. Moseley, S. Shepherd, D.J. Fulton, B.D. Sinclair, M.H. Dunn, Phys. Rev. A **50**, 4339 (1994)
15. S. Jin, Y. Li, M. Xiao, Opt. Commun. **119**, 90 (1995)
16. A. Ray, MdS Ali, A. Chakrabarti, Eur. Phys. J. D **67**, 78 (2013)
17. A. Ray, MdS Ali, A. Chakrabarti, Opt. Laser Technol. **60**, 107 (2014)
18. A. Ray, MdS Ali, A. Chakrabarti, Eur. Phys. J. D **69**, 41 (2015)
19. B.W. Shore, Acta Phys. Slov. **58**, 243 (2008)
20. J.C. Garrison, R.Y. Chiao, *Quantum Optics. Reprint* (Oxford University Press, Oxford, 2009)
21. R. Loudon, Opt. Commun. **49**, 67 (1984)
22. H.P. Yuen, Phys. Rev. A **13**, 2226 (1976)
23. S.R. Senitzky, J. Opt. Soc. Am. B **1**, 879 (1984)
24. <http://steck.us/alkalidata/rubidium87numbers.pdf>. version 2.1.5. Accessed 13 Jan 2015
25. M.S. Safronova, C.J. Williams, C.W. Clark, Phys. Rev. A **69**, 022509 (2004)
26. Daniel J. Whiting, James Keaveney, Charles S. Adams, Ifan G. Hughes, Phys. Rev. A **93**, 043854 (2016)
27. H.S. Moon, Opt. Commun. **284**, 1327 (2011)
28. Y.-Q. Li, M. Xiao, Opt. Lett. **20**, 1489 (1995)
29. I.G. Hughes, T.P.A. Hase, *Measurements and Their Uncertainties* (Oxford University Press, Oxford, 2010)
30. M.O. Scully, M.S. Zubairy, *Quantum Optics, Sixth Printing* (Cambridge University Press, Cambridge, 2008)
31. Z. Ficek, B.J. Dalton, P.L. Knight, Phys. Rev. A **51**, 4062 (1995)
32. D. Felinto, A.Z. Khoury, S.S. Vianna, Phys. Lett. A **319**, 448 (2003)
33. M. Das, B. Sen, A. Ray, A. Pathak (2016). [arXiv:1608.01781](https://arxiv.org/abs/1608.01781)